



Stress-modulated driving force for lithiation reaction in hollow nano-anodes



Zheng Jia, Teng Li*

Department of Mechanical Engineering, University of Maryland, College Park, MD 20742, USA

HIGHLIGHTS

- We determine the effect of mechanical stress on driving force for lithiation reaction.
- We consider concurrent lithiation reaction and deformation with a sharp reaction front.
- We reveal a hollow silicon nanowire is easier to be fully lithiated than a solid one.

ARTICLE INFO

Article history:

Received 8 September 2014
 Received in revised form
 24 October 2014
 Accepted 16 November 2014
 Available online 18 November 2014

Keywords:

Silicon anodes
 Lithiation reaction
 Driving force
 Lithium ion battery
 Stress

ABSTRACT

Lithiation of a crystalline silicon anode proceeds by the movement of an atomically sharp reaction front that separates a pristine crystalline phase and a fully-lithiated amorphous phase. The velocity of the reaction front is limited rather by the reaction rate at the lithiation front than by the diffusivity of lithium ions in the amorphous lithiated phase. Experiments on solid nanoparticle/nanowire silicon anodes show an initial rapid advancing of reaction front at the initial stage of lithiation, followed by an apparent slowing or even halting of the reaction front propagation. Lithiation-induced stresses during lithiation are attributed to alter the driving force of lithiation and thus result in the observed slowing of reaction front. Recent experiments on lithiation of hollow silicon nanowires reveals similar slowing of reaction front, however, quantitative study of the effect of lithiation-associated stress on the driving force of lithiation still lacks so far. Here, through chemo-mechanical modeling and theoretical formulation, we present a comprehensive study on lithiation-induced stress field and its contribution to the driving force of lithiation reaction in hollow silicon nanowire anodes. We show that hollow silicon nano-anodes could be fully lithiated with lower stress-induced energy barrier than solid silicon nano-anodes. As a result, it is expected that the hollow nanowires and nanoparticles may serve as an optimal structural design for high-performance anodes of lithium-ion batteries. Results from the present study shed light on a number of open questions of lithiation kinetics of silicon-based anodes in recent literature and offer insight on developing silicon-based anodes with high charging capacity and high charging rate.

© 2014 Elsevier B.V. All rights reserved.

1. Introduction

There has been a surge of interests in developing next-generation lithium-ion batteries with high specific capacity [1–5]. Silicon is emerging as the most promising anode (i.e., negative electrode¹) material due to its high specific capacity which is about ten times that of current graphite-based anodes [6,7]. The high

theoretical capacity of silicon stems from the fact that one silicon atom can host up to 3.75 lithium atoms upon fully lithiation [8]. However, on the other hand, insertion of large amount of lithium atoms causes excessive volume change (~300%) and large mechanical stresses, which may eventually fracture the silicon anodes and lead to huge irreversible capacity fading [9–11]. Therefore, mechanical failures induced by the large volumetric expansion during lithiation are the key issue that hinders the mass application of silicon as anodes for next-generation lithium-ion batteries. To mitigate the mechanical failures of silicon-based anodes, intensive research efforts have been focused on developing nanostructured anodes including nanowires [9,12], nano-sized thin film [13], nanoporous structures [14,15], nano-sized beaded-string structure

* Corresponding author.

E-mail address: lit@umd.edu (T. Li).

¹ The term of “anode” here corresponds to the discharging half-cycle in electrochemistry. Silicon indeed serves as the cathode during the charging half-cycle. In either half-cycle, silicon is the negative electrode.

[16], nano-walls [17] and nano-islands [18,19]. Lithiation-induced stress, deformation and mechanical failure in these novel silicon nanostructures are widely studied through experimental characterization [20–22] and chemo-mechanical modeling [23–30]. As shown in these studies, shape optimization, mechanical constraint and size control help release excessive lithiation-induced stresses and thus avoid pulverization of anodes and active materials in nano-structured silicon anodes [16,23,24,31].

Lithiation kinetics in such silicon nanostructured anodes has also been studied recently [25,32,33]. Experimental evidences have accumulated that the lithiation of crystalline silicon advances by the movement of an atomically-sharp reaction front [12,27,33,34], which separates an unlithiated pristine silicon phase and a fully lithiated silicon phase (as shown by the schematics of Fig. 1(b)). Therefore, the lithiation of silicon is a two-phase reaction [35,36] and it indicates that the lithiation process is controlled by the reaction between lithium and silicon at the reaction front, rather than the diffusion of lithium through the lithiated silicon phase [25,27]. Experimental measurements of reaction velocity in solid silicon particles reveal that the reaction front usually slows down as it progresses into the solid particles [32]. Existing studies have shown that lithiation-induced stress field could affect the driving force of lithiation [21,22,28,37,38]. A theoretical model is recently developed to account for simultaneous lithiation and the associated stress field evolution [25,31]. Interestingly, the model predicts that the evolving stress field across the reaction front acts as an energy barrier and retards the lithiation reaction. Therefore, it is expected that the contribution of stresses to the driving force for Li–Si reaction results in the observed slowing of reaction front in solid particle silicon anodes [25,32].

Recently, hollow silicon nano-anodes attract attentions since they have more free space to accommodate the large volume expansion due to lithium insertion and thus possess excellent cycling performance [15,39–43]. It is noteworthy that lithiation of hollow silicon nanowires also shows similar slowing or even halting of the reaction front [16]. Although the observed slowing or halting of reaction front in hollow silicon anodes can also be attributed to the negative contribution of lithiation-induced stress, a quantitative understanding is still lacking to fully decipher the lithiation-induced stress field and its influence on reaction rate in hollow silicon nano-anodes. What remain elusive include, e.g., how does the hollow nature of silicon anodes alter the role of mechanical stresses in retarding lithiation reaction? How does the

slowing of reaction front in hollow silicon anodes differ from that in solid ones? Is hollow nanostructure a good anode design from lithiation kinetics standpoints? Quantitative answers to these questions are crucial for advancing the design of high-performance silicon-based hollow anodes.

In this paper, we present a finite element based chemo-mechanical modeling method as well as a theoretical model to quantitatively determine the stress field in hollow silicon nanowire anodes as the lithiation reaction proceeds. The driving force for the movement of the sharp lithiation reaction front is then identified based on the stress distribution across the sharp reaction front. The lithiation process is fully specified by the current position of the lithiation front and the lithiation-induced volume expansion of the fully lithiated silicon. Our calculation reveals that, compared with solid silicon anodes, hollow silicon anodes suffer less stress-induced reduction of driving force for lithiation, therefore could act as a better anode structural design for next-generation high performance lithium-ion batteries. Moreover, our calculation results can help answer a number of open questions of lithiation kinetics of silicon-based anodes in perspective of the experimental results in recent literature.

2. Lithiation-induced stress field in a hollow nanowire

We consider the lithiation process of a hollow cylindrical amorphous silicon nanowire anode with an inner radius R_i and outer radius R_o at the pristine reference state, whose cross-section view is illustrated in Fig. 1(a). Recent experiments indicate that the reaction rate of amorphous silicon at the lithiation front is isotropic, without obvious preferential directions [16]. Therefore, as lithiation advances, velocity of the reaction front is the same everywhere along the front and thus the lithiation front sweeps through the hollow silicon nanowire with a cylindrical shape of radius $A(t)$ (Fig. 1(a)). Here, $A(t)$ decreases with time as the reaction front propagates from the outer surface of silicon nanowire to its inner surface. During this process, lithiated silicon expands in volume to accommodate the lithium insertion. Therefore, a material element characterized by initial radius R in the reference state is deformed and moves to a new position with radius $r(t)$ after this material element is lithiated. In particular, the outer surface with a radius R_o in the reference state is pushed out to be the current outer surface with a radius r_o . During the lithiation process, stress field arises and evolves in response to the volume change caused by lithium insertion.

To solve the lithiation-induced stress field in the silicon nanowire, the concurrent lithiation reaction and deformation of the silicon nanowire along its cross-section are simulated using finite element code ABAQUS. In order to mimic the inward movement of the reaction front, the cross section of the silicon nanowire is evenly divided into N (an integer) annuluses and these annuluses are lithiated one by one from outer surface toward inner core of the silicon nanowire. Experimental evidence has accumulated that the reaction front is atomically sharp with thickness of ~ 1 nm [34]. In the simulation, the thickness of the reaction front is defined by the thickness of each annulus, which is set to be 2 nm to compromise between simulation expense and modeling fidelity. The lithiation of each annulus is modeled by prescribing a volume change of 400% (i.e., fully lithiated). The pristine silicon is modeled to be linearly elastic with a Young's modulus of 160 GPa and a Poisson's ratio of 0.24 [27]. The fully lithiated silicon phase is taken to be elastic-perfectly plastic with a Young's modulus of 40 GPa, a Poisson's ratio of 0.22 and a yielding stress of 1.5 GPa [27,44]. Recent experiments reveal that a hollow cylindrical silicon anode with the deformation of its inner surface largely constrained demonstrates a better durability during lithiation compared with its counterpart

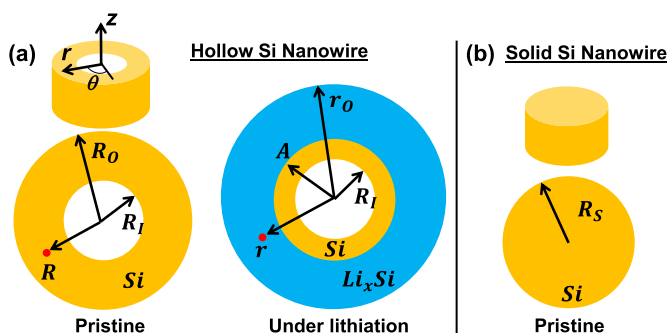


Fig. 1. (a) Left: cross-section of a pristine hollow cylindrical silicon nanowire with an initial inner radius R_i and an initial outer radius R_o is considered to be the reference state. A material point (labeled by the red dot) is at a radius R . Right: in the lithiation state at time t , the lithiation front is located at a radius of $A(t)$, the outer surface is now at a radius $r_o(t)$, and the material point labeled by R in the reference state moves to a new location at a radius $r(t)$. (b) Cross-section of a pristine solid cylindrical silicon nanowire of a radius R_s , with the same volume of the hollow silicon nanowire defined in (a). (For interpretation of the references to color in this figure legend, the reader is referred to the web version of this article.)

with its inner surface free to deform. To study such a boundary effect on the lithiation-induced stress field, we perform chemo-mechanical simulations with two types of boundary conditions of the inner surface of the hollow silicon nanowire: traction-free and fixed. In all simulations, the outer surface of the silicon nanowire is traction-free, simulating the lithiation of the silicon nanowire without external lateral constraint as suggested in *in situ* experiments. To clarify how the hollow geometry affects the lithiation process, we compare the lithiation of hollow silicon nanowires with different inner radii but same volume with that of a solid silicon nanowire of the same volume, i.e., $R_0^2 - R_I^2 = R_S^2$ (Fig. 1). To facilitate the comparison among various lithiation stages, in all results reported hereinafter, all stress components are plotted as a function of radial location in the reference configuration (i.e., pristine state) and all length dimensions are normalized by R_S .

Fig. 2(a–f) plots the finite element simulation results on the distribution of three stress components (i.e., radial stress σ_r , hoop stress σ_θ , and axial stress σ_z , all normalized by the yield stress of fully lithiated silicon σ_Y) along the radial direction of a hollow silicon nanowire, for three stages of lithiation process with the reaction front being at $A/R_S = 1.04$, 0.86, and 0.58, respectively. The

inner and outer radii of the hollow silicon nanowire is 50 nm and 111.8 nm respectively, with a corresponding solid nanowire of radius $R_S = 100$ nm. Fig. 2 shows tri-axial nature of the lithiation-induced stress field in various stages. When the inner surface of the hollow silicon nanowire is free (Fig. 2 (a–c)), it is shown that compressive stresses accumulate in the unlithiated pristine silicon core along both radial and hoop directions with radial stress vanishing at the inner surface due to the traction-free boundary condition. The unlithiated core experiences increasing compressive radial/hoop stresses as lithiation advances.

Axial stress σ_z is constant in the unlithiated silicon core, being tensile at the early stage of lithiation, gradually decreasing to be zero as lithiation advances. In Fig. 2(b) and (c), a discontinuity in hoop stress σ_θ and axial stress σ_z exists across the lithiation front due to the abrupt change of material properties from pristine silicon to fully lithiated phase ($Li_{3.75}Si$). At the reaction front, the constraint from the inner unlithiated core acts against the lithiation-induced volume expansion of the $Li_{3.75}Si$ phase. As a result, the $Li_{3.75}Si$ phase at the reaction front is under compressive stresses σ_θ and σ_z ; and the resulting von Mises stress readily exceeds the yielding strength, causing yielding of the fully lithiated

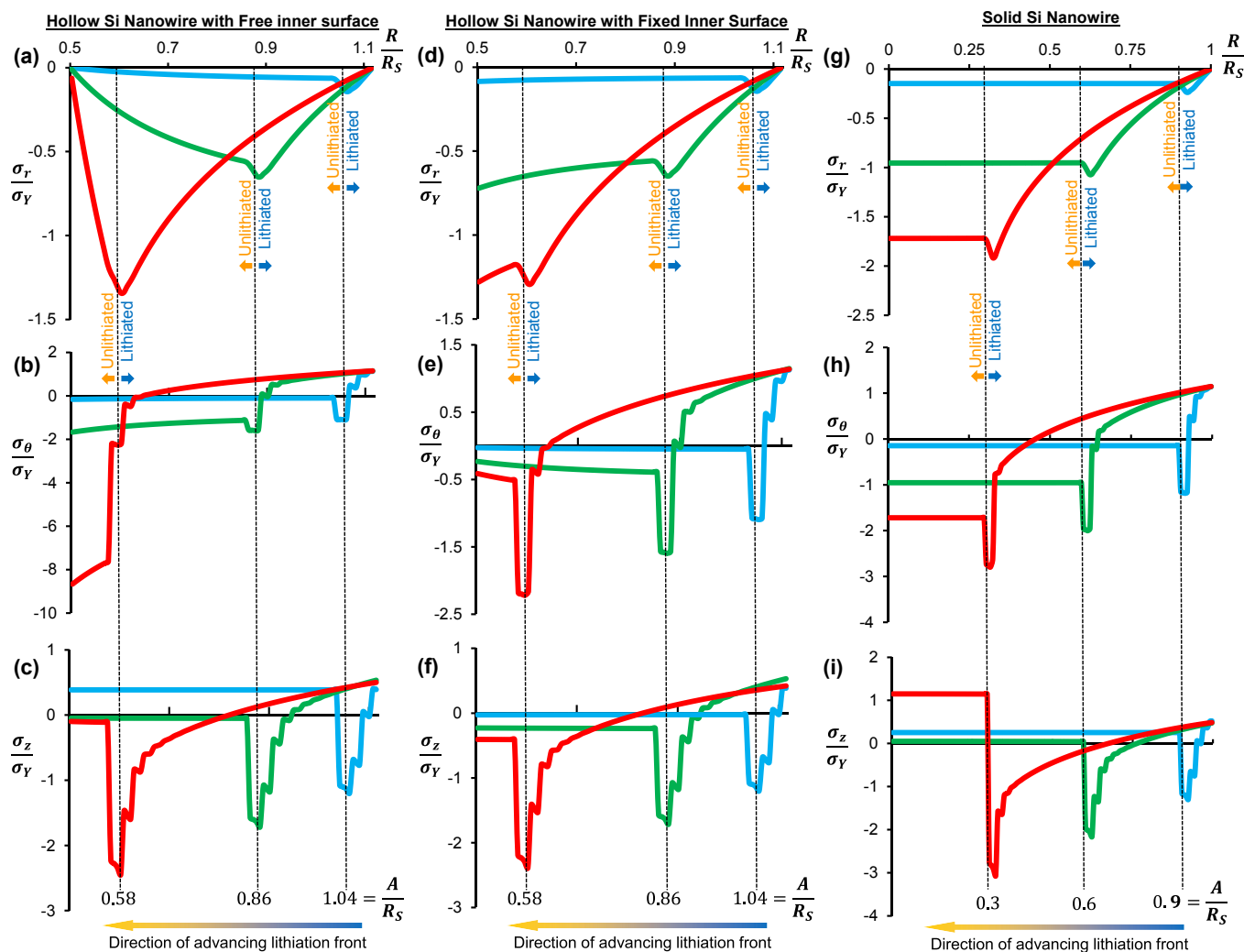


Fig. 2. Finite element simulation results on lithiation-induced stress field in a hollow silicon nanowire with a traction-free inner surface (a–c), with a fixed inner surface (d–f) and that in a solid silicon nanowire (g–i). In the hollow silicon nanowire, distributions of radial stress σ_r (a, d), hoop stress σ_θ (b, e) and axial stress σ_z (c, f) are shown for various reaction front positions (depicted by a dashed line) of $A/R_S = 1.04$ (blue curve), $A/R_S = 0.86$ (green curve) and $A/R_S = 0.58$ (red curve). In the solid silicon nanowire, distributions of radial stress σ_r (g), hoop stress σ_θ (h) and axial stress σ_z (i) are shown for reaction front positions (depicted by a dashed line) of $A/R_S = 0.9$ (blue curve), $A/R_S = 0.6$ (green curve) and $A/R_S = 0.3$ (red curve). (For interpretation of the references to color in this figure legend, the reader is referred to the web version of this article.)

silicon phase on the reaction front. In the outer lithiated shell, due to the “pushing-out” effect, the $Li_{3.75}Si$ phase undergoes elastic unloading and the hoop stress σ_θ gradually becomes tensile inside the lithiated shell and eventually reaches σ_Y at the external surface of the anode, which may induce fracture nucleating at the nanowire surface as reported for solid crystalline nanopillar in literature. When the inner surface of the hollow silicon nanowire is fixed (Fig. 2(d–f)), the constraint at its inner surface strongly affects the stress distribution within the unlithiated silicon core by setting a non-trivial compressive radial stress σ_r at the inner surface of hollow nanowire but effectively reducing the compressive hoop stress σ_θ . On the other hand, the stress distribution in the lithiated shell is rather close to that in a hollow nanowire with a free inner surface.

For comparison, Fig. 2(g–i) plots the distributions of stress components in a solid silicon nanowire with the same volume as the hollow one in Fig. 2(a–f), at various reaction front stages. In the solid silicon nanowire, stress profiles in the lithiated shell and on the reaction front are similar to those in the hollow nanowire. However, the stress distribution and evolution in the solid unlithiated core strongly differ from those observed in the hollow nanowire. As shown in Fig. 2(g) and (h), the solid unlithiated core experiences in-plane hydrostatic compression with a constant distribution of radial stress σ_r and hoop stress σ_θ ($\sigma_r = \sigma_\theta$). More importantly, it is also noted that the axial stress σ_z within the unlithiated core decreases slightly when the reaction front propagates into the nanowire; but increases significantly when the reaction front approaches the center of the nanowire (Fig. 2(i)). Such a trend can be understood as: during lithiation the pristine core is stretched axially due to the swelling of the lithiated shell and thus experiences tensile axial stress. The stretch effect becomes rather substantial when the reaction front is close to the center of the nanowire: the tension in the unlithiated core with an ever-decreasing cross-section needs to balance the compression in the outer lithiated part with an ever-increasing cross-section. As a result, significant tensile axial stress builds up in the pristine core, which could be high enough to cause the cracking in the unlithiated core as observed in recent experiments [16].

As an effort to validate the simulated results shown above, we developed a theoretical mechanics model of the lithiation-induced stress field in a hollow silicon nanowire. Such a model can be readily reduced to solve the stress field in a solid silicon nanowire. Zhao et al. recently established a theoretical formulation of concurrent reaction and plasticity to investigate the lithiation of a hollow nanowire with its outer surface confined by a rigid solid-electrolyte interphase layer [31]. In their theoretical model, the diffusion of lithium in silicon is assumed to be fast enough to allow for a uniform distribution of lithium, and as a result, lithiation front is not involved in the model and the lithiation process is fully specified by the lithiation-induced uniform volume expansion of the silicon. To further clarify the underpinning mechanism of lithiation-induced stresses associated with the evolving sharp lithiation front, here we present the lithiation-induced stress field obtained from a theoretical formulation. Distinct from previous works, our theoretical formulation considers both concurrent movement of reaction front and volume expansion induced by lithium insertion at the reaction front. Detailed description of the theoretical mechanics model is given in the Appendix.

As illustrated in the Fig. 1(a), the cross section of the Si nanowire under lithiation can be subdivided into three regions: the fully lithiated silicon shell ($A < r \leq r_0$), the reaction front ($r = A$) and the unlithiated pristine silicon core ($R_l < r < A$).

As abovementioned, in the lithiated silicon shell, the current position of a material point r is given by $r = \sqrt{A^2 + \beta(R^2 - A^2)}$, here

β is the volume expansion ratio defined by the volume of the lithiated silicon $Li_{3.75}Si$ over that of the pristine silicon. Then the current outer radius $r_0 = \sqrt{A^2 + \beta(R_0^2 - A^2)}$. The stress distribution in the lithiated silicon shell can be solved by considering the concurrent lithiation and plasticity.

$$\sigma_r = \frac{2}{\sqrt{3}}\sigma_Y \log\left(\frac{r}{r_0}\right), \quad (A < r \leq r_0) \quad (1)$$

$$\sigma_\theta = \frac{2}{\sqrt{3}}\sigma_Y + \frac{2}{\sqrt{3}}\sigma_Y \log\left(\frac{r}{r_0}\right), \quad (A < r \leq r_0) \quad (2)$$

$$\sigma_z = \frac{1}{\sqrt{3}}\sigma_Y + \frac{2}{\sqrt{3}}\sigma_Y \log\left(\frac{r}{r_0}\right), \quad (A < r \leq r_0) \quad (3)$$

Where σ_r , σ_θ and σ_z represent the radial stress, hoop stress and axial stress, respectively. σ_Y is the yielding stress of the fully lithiated silicon $Li_{3.75}Si$. Therefore, at the outer surface of the silicon nanowire $r = r_0$, the hoop stress $\sigma_\theta(r_0, t) = 2/\sqrt{3}\sigma_Y > 0$ (tensile), which agrees with the experimentally observed cracks at the outer surface of the lithiated Si anodes [45].

Right on the lithiation front, the radial stress σ_r is continuous across the lithiation front, therefore, according to Eq. (1), the radial stress at the lithiation front $r = A$ is

$$\sigma_r = \frac{2}{\sqrt{3}}\sigma_Y \log\left(\frac{A}{r_0}\right) \quad (4)$$

and we also have

$$\sigma_\theta = -\sigma_Y + \frac{2}{\sqrt{3}}\sigma_Y \log\left(\frac{A}{r_0}\right) \quad (5)$$

$$\sigma_z = -\sigma_Y + \frac{2}{\sqrt{3}}\sigma_Y \log\left(\frac{A}{r_0}\right) \quad (6)$$

In the unlithiated pristine Si core, as discussed above, the inner surface of the remaining unlithiated silicon is either under fixed boundary condition (if the hollow nanowire is bonded to an inner constraint) or traction-free (if the hollow nanowire is free-standing). The stress field in the pristine unlithiated silicon can be obtained by solving a Lamé problem. For the traction-free inner surface, the stress field ($R_l \leq r < A$) is given as

$$\sigma_r = \frac{2}{\sqrt{3}}\sigma_Y \log\left(\frac{A}{r_0}\right) \frac{A^2}{A^2 - R_l^2} \left(1 - \frac{R_l^2}{r^2}\right), \quad (R_l \leq r < A) \quad (7)$$

$$\sigma_\theta = \frac{2}{\sqrt{3}}\sigma_Y \log\left(\frac{A}{r_0}\right) \frac{A^2}{A^2 - R_l^2} \left(1 + \frac{R_l^2}{r^2}\right), \quad (R_l \leq r < A) \quad (8)$$

$$\sigma_z = \frac{4\nu}{\sqrt{3}}\sigma_Y \log\left(\frac{A}{r_0}\right) \frac{A^2}{A^2 - R_l^2}, \quad (R_l \leq r < A) \quad (9)$$

Similarly, fixed boundary condition at the inner surface gives a stress field ($R_l \leq r < A$) as follows

$$\sigma_r = \frac{2}{\sqrt{3}}\sigma_Y \log\left(\frac{A}{r_0}\right) \left[\frac{1}{\frac{r^2}{A^2} + \frac{1}{(1-2\nu)R_l^2}} + \frac{1}{\frac{(1-2\nu)R_l^2}{A^2} + 1} \right], \quad (R_l \leq r < A) \quad (10)$$

$$\sigma_{\theta} = \frac{2}{\sqrt{3}} \sigma_Y \log \left(\frac{A}{r_0} \right) \left[\frac{1}{\frac{r^2}{A^2} + \frac{1}{(1-2\nu)R_I^2}} + \frac{1}{\frac{(1-2\nu)R_I^2}{A^2} + 1} \right], \quad (R_I \leq r < A) \quad (11)$$

$$\sigma_z = \frac{4\nu}{\sqrt{3}} \sigma_Y \log \left(\frac{A}{r_0} \right) \frac{1}{\frac{(1-2\nu)R_I^2}{A^2} + 1}, \quad (R_I \leq r < A) \quad (12)$$

where $\nu = 0.24$ is the Poisson's ratio of pristine amorphous silicon.

Based on Eqs. (1–12), Fig. 3 plots the theoretical results on the distribution of radial stress σ_r , hoop stress σ_{θ} , and axial stress σ_z , along the radial direction of the hollow silicon nanowire, for three stages of lithiation process with the reaction front being at $A/R_S = 1.04, 0.86,$ and $0.58,$ respectively. The same geometric parameters of the hollow silicon nanowire and its solid counterpart as in finite element simulations (e.g., in Fig. 2) are used here. For the case of silicon nanowire with a free inner surface, distribution of

radial stress σ_r (Fig. 3(a)) and hoop stress σ_{θ} (Fig. 3(b)) agree reasonably well with the prediction from finite element simulations (Fig. 2(a) and (b), respectively). The jump of hoop stress between a material point on the lithiation front and its neighboring material point in the fully lithiated shell results from neglecting the trivial elastic deformation in the lithiated phase. Moreover, the distribution of axial stress σ_z outside the unlithiated core (Fig. 2(c), e.g., on the right of each dashed line) also well reproduces the finite element simulation results presented in Fig. 2(c). However, the theoretical mechanics model predicts an increasing compressive axial stress inside the unlithiated core (Fig. 2(c), e.g., on the left of each dashed line) as the lithiation advances. This is different from the prediction from finite element simulation as shown in Fig. 2(c). Such a discrepancy might result from the assumption of plane-strain conditions adopted in the theoretical mechanics model, which could indeed constrain the modest axial elongation of the silicon nanowire under lithiation.

For the case of silicon nanowire with a fixed inner surface, the theoretical mechanics model results (Fig. 3(d–f)) match

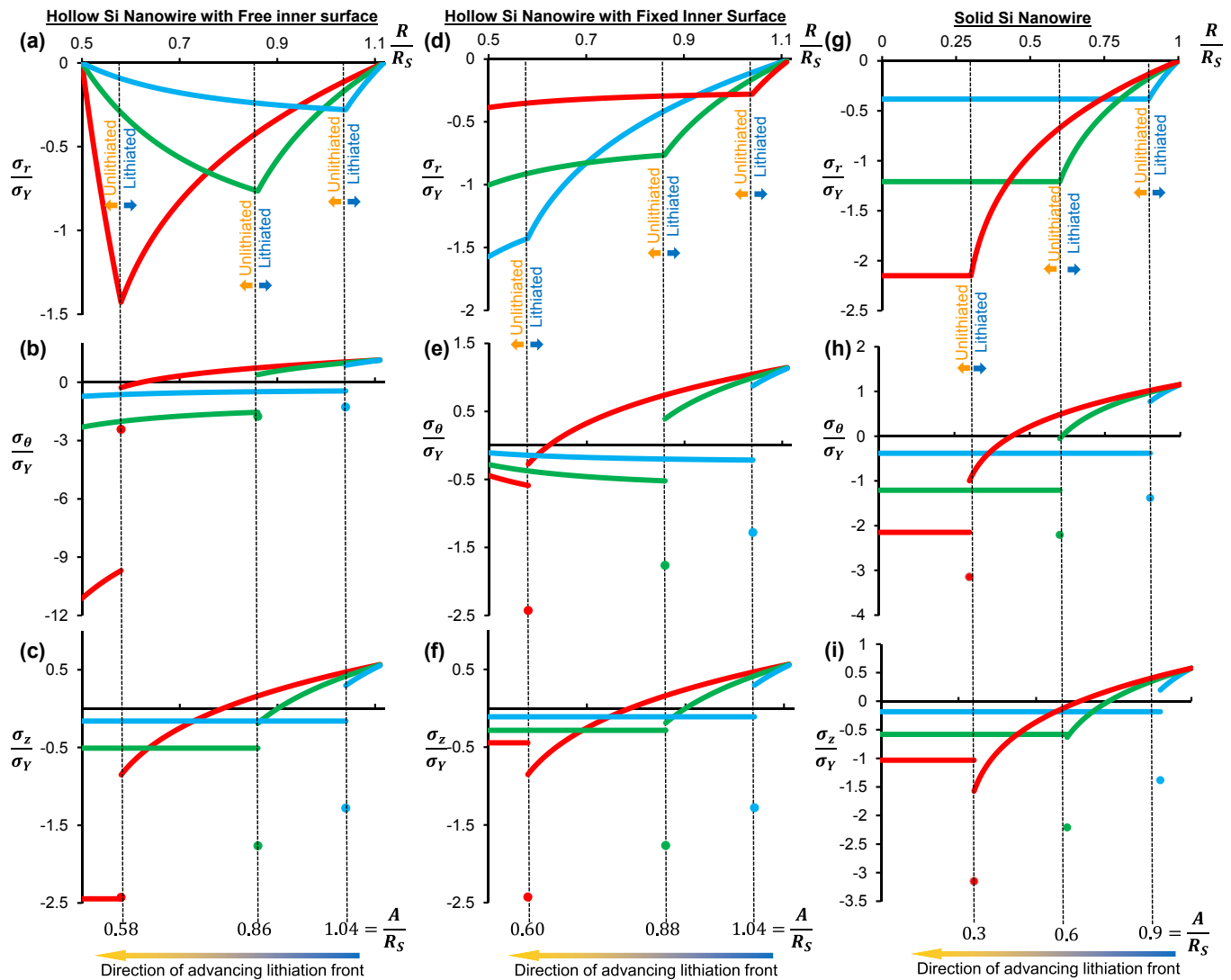


Fig. 3. Theoretical mechanics model results on lithiation-induced stress field in a hollow silicon nanowire with a traction-free inner surface (a–c), with a fixed inner surface (d–f) and that in a solid silicon nanowire (g–i). In the hollow silicon nanowire, distributions of radial stress σ_r (a, d), hoop stress σ_{θ} (b, e) and axial stress σ_z (c, f) are shown for various reaction front positions (depicted by a dashed line) of $A/R_S = 1.04$ (blue curve), $A/R_S = 0.86$ (green curve) and $A/R_S = 0.58$ (red curve). In the solid silicon nanowire, distributions of radial stress σ_r (g), hoop stress σ_{θ} (h) and axial stress σ_z (i) are shown for reaction front positions (depicted by a dashed line) of $A/R_S = 0.9$ (blue curve), $A/R_S = 0.6$ (green curve) and $A/R_S = 0.3$ (red curve). (For interpretation of the references to color in this figure legend, the reader is referred to the web version of this article.)

remarkably well with those obtained by finite element simulations (Fig. 2(d–f)). In such a case, the fixed inner surface constrains the free expansion of the silicon nanowire in its axial direction, which in turn makes the assumption of plane-strain conditions reasonable and accurate. For the case of solid silicon nanowire, theoretical derivation with the assumption of plane-strain conditions leads to an increase in the compressive axial stress in the un lithiated core as the reaction front migrates towards the center of the nanowire (Fig. 3(i)), which is contrary to the abovementioned finite element simulation results and experimental findings [16]. The theoretical prediction of the radial and hoop stresses in the un lithiated core (Fig. 3(g, h)) agrees reasonably with the finite element simulation results, but with a slightly more compressive stress level. Nonetheless, as will be shown in the next section, both the finite element simulations and theoretical model analysis presented above can capture the key features of the distribution and evolution of lithiation-induced stress in both hollow and solid silicon nanowires that govern the contribution of mechanical stress to the driving force of lithiation reaction, the focus of the present paper.

Both finite element simulations and theoretical mechanics model predict the interplay between the concurrent reaction and plasticity during lithiation of the silicon nanowire and reveal the three dimensional nature of the resulting stress field in the nanowire. In particular, we show that the resulting stress and deformation fields in the hollow silicon nanowire can be fully determined once the position of the lithiation front is given. Recent studies show that reaction kinetics is dictated by the stress field within the un lithiated core and right on the reaction front [25,32]. As shown above, since the stress field within the un lithiated core is highly affected by the boundary conditions at the inner surface of the hollow silicon nanowire, it is expected that such boundary conditions would significantly influence the lithiation kinetics of the silicon nanowire. In next section, we report detailed study of the effect of the lithiation-induced stress on the driving force for lithiation reaction.

3. Effect of stress on driving force for lithiation

The reaction at lithiation front advances by transforming lithium and silicon into a lithiated phase, as described by the chemical reaction equation, $Li + 1/xSi = 1/xLi_xSi$. The driving force for such a reaction to proceed represents the net change of the free energy associated with the reaction, which can be given by

$$\Delta G = \Delta G_{\text{intrinsic}} - e\Phi + \Delta G_{\text{stress}}, \quad (13)$$

where $\Delta G_{\text{intrinsic}}$ represents the free energy change due to lithiation reaction without any applied voltage and stress, which intrinsically takes a negative value (i.e., energetically favorable). For example, $\Delta G_{\text{intrinsic}} = -0.18$ eV for $Li_{2.1}Si$; $-e\Phi$ denotes the external work done by the applied voltage Φ ; and ΔG_{stress} represents the contribution of mechanical stress on the driving force for lithiation reaction. A negative ΔG drives the reaction while a positive one stalls the reaction. Moreover, a more negative ΔG represents a higher driving force and a more positive ΔG denotes more resistance to lithiation.

The contribution of lithiation-induced stresses to the lithiation driving force can be computed by

$$\Delta G_{\text{stress}} = \frac{1}{x} \left(\sigma_m^{Si} \Omega^{Si} - \sigma_m^{Li_xSi} \Omega^{Li_xSi} \right), \quad (14)$$

where Ω^{Si} and Ω^{Li_xSi} represent the atomic volumes of Si and Li_xSi , respectively (note that $\Omega^{Li_xSi} = \beta \Omega^{Si}$); σ_m^{Si} and $\sigma_m^{Li_xSi}$ denote the mean stress (i.e., $1/3(\sigma_r + \sigma_\theta + \sigma_z)$) in the remaining un lithiated silicon and the mean stress on the lithiation front, respectively.

Fig. 4 plots ΔG_{stress} as a function of the lithiation front position A/R_S , for a solid silicon nanowire and hollow silicon nanowires of the same volume as the solid one but with various inner radii, using the finite element simulation results of lithiation-induced stresses (e.g., as in Fig. 2).

For a solid silicon nanowire, ΔG_{stress} is always positive and monotonically increases as the reaction advances (Fig. 4(a)). For example, $\Delta G_{\text{stress}} \approx 0.81$ eV when $A/R_S = 0.03$ (very close to fully lithiation), which is significantly higher than the intrinsic driving force for lithiation reaction $\Delta G_{\text{intrinsic}}$. In other words, lithiation-induced stress could potentially severely retard or even halt the lithiation reaction in a solid silicon nanowire.

For a hollow silicon nanowire, (e.g., Fig. 4(c) for the one corresponding to Fig. 2), at the initial stage of lithiation reaction, ΔG_{stress} is positive and increase monotonically with a slope modestly lower than that for a solid nanowire as the reaction advances. There is negligible difference between the two cases of boundary conditions at the inner surface of the nanowire. However, in later stage of lithiation reaction, the change of ΔG_{stress} as the reaction proceeds further shows distinct trends for the two cases of boundary conditions at the inner surface of the nanowire. With a fixed inner surface of the nanowire, ΔG_{stress} continues increase monotonically, in a rather linear fashion. For example, $\Delta G_{\text{stress}} \approx 0.38$ eV when $A/R_S = 0.53$ (very close to fully lithiation, reaching the last virtual annulus in simulation). By contrast, with a free inner surface, ΔG_{stress} reaches its peak value of ~ 0.28 eV at an intermediate lithiation stage ($A/R_S = 0.67$), and then decreases monotonically as the reaction advances toward the inner surface, becoming negative (~ -0.1 eV) as approaching full lithiation. The above results suggest that at the later stage of lithiation reaction, a free inner surface of hollow silicon nanowires can indeed facilitates the lithiation reaction by increasing the driving force, which can be further understood as follows. As shown in Fig. 2, at the later stage of lithiation reaction, the level of the three principal stress components, thus the level of mean stress on the lithiation front $\sigma_m^{Li_xSi}$ is comparable for both cases of boundary conditions at the inner surface. On the other hand, the compressive hoop stress σ_θ in the remaining un lithiated silicon of the nanowire with a free inner surface reaches a level ($\sigma_\theta/\sigma_\gamma \approx -8$) substantially higher than not only the other two principal stress components, but also the hoop stress on the lithiation front ($\sigma_\theta/\sigma_\gamma \approx -2$). As a result, the mean stress in the un lithiated silicon σ_m^{Si} becomes so negative that the first term in Eq. (14) overbalances the second term, leading to a negative ΔG_{stress} .

Further comparison among hollow nanowires with the same volume but different inner radii (Fig. 4(b–d)) shows that a hollow nanowire anode with a larger inner radius experiences lower stress-induced resistance to lithiation reaction at its early stage, regardless the boundary conditions at the inner surface, and could have even higher driving force for lithiation reaction toward its final stage if the inner surface of the nanowire is free.

ΔG_{stress} can also be explicitly solved using the theoretical formulation delineated in Section 2. For example, the driving forces associated with lithiation-induced stress in a hollow silicon nanowire with traction-free inner surface and fixed inner surface can be given by

$$\Delta G_{\text{stress}}^{\text{traction-free}} = \frac{2\sigma_\gamma \Omega^{Si}}{x} \left[\frac{2}{3\sqrt{3}} \log \left(\frac{A}{r_0} \right) \frac{(1+\nu)A^2}{A^2 - R_I^2} - \frac{\beta}{\sqrt{3}} \log \left(\frac{A}{r_0} \right) + \frac{\beta}{3} \right] \quad (14.1)$$

and

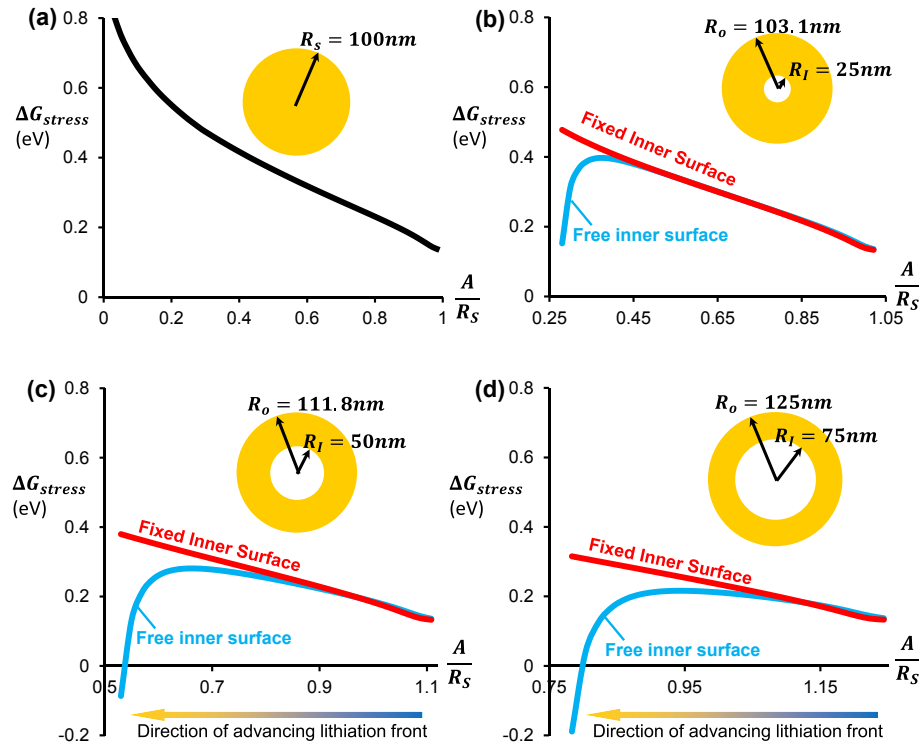


Fig. 4. Finite element simulation results on stress-modulated driving force for lithiation as a function of the lithiation front position A/R_s , for (a) a solid silicon nanowire and (b–d) hollow silicon nanowires with normalized inner radius of (b) $R_i/R_s = 0.25$, (c) $R_i/R_s = 0.5$ and (d) $R_i/R_s = 0.75$, respectively. Blue lines in (b–d) represent the case of a hollow nanowire with a traction-free inner surface and red lines represent the case of a hollow nanowire with a fixed inner surface. (For interpretation of the references to color in this figure legend, the reader is referred to the web version of this article.)

$$\Delta G_{\text{stress}}^{\text{fixed}} = \frac{2\sigma_Y \Omega^{\text{Si}}}{x} \left[\frac{2}{3\sqrt{3}} \log\left(\frac{A}{r_0}\right) \frac{(1+\nu)A^2}{(1-2\nu)R_i^2 + A^2} - \frac{\beta}{\sqrt{3}} \log\left(\frac{A}{r_0}\right) + \frac{\beta}{3} \right], \quad (14.2)$$

respectively. Eqs. (14.1) and (14.2) are plotted in Fig. 5(b–d) for the same anode structures as in Fig. 4. Here, we take $\beta = 4$, $x = 3.75$, $\Omega^{\text{Si}} = 2 \times 10^{-29} \text{ m}^3$ and $\sigma_Y = 1.5 \text{ GPa}$. The prediction of stress-modulated driving force for lithiation reaction from theoretical mechanics model shows reasonable agreement with that from finite element simulations, with a modestly higher level of ΔG_{stress} values, resulting from the slight difference in the predicted lithiation-induced stresses as explained in Section 2.

Nonetheless, both finite element simulations and theoretical mechanics model predict that a hollow silicon nanowire anode can be fully lithiated more easily than a solid one with the same volume, due to reduced resistance to reaction associated with lithiation-induced stress.

4. Discussion

The quantitative results in this paper can shed light on a number of open questions about the lithiation kinetics of silicon-based anodes in recent literature. For example:

Sun et al. observed the slowing and subsequent halting of the reaction front in hollow silicon nanowire under lithiation [16]. Based on our results presented above, such a phenomenon is mainly due to the stress-modulated driving force for lithiation reaction at the reaction front: for a hollow silicon anode with free-inner surface (as indicated in Figs. (4) and (5)), stress-associated

resistance for reaction gradually builds up as lithiation advances and peaks at a certain reaction front position. Such an increasing resistance for reaction may result in the observed slowing of reaction front. Moreover, it is worth noting that the hollow nanowires in Ref. [16] have a negligible inner radius of 3 nm, compared to the outer radius of 53 nm. As predicted in Figs. 4 and 5, a smaller inner radius leads to a higher stress-associated resistance for reaction. Therefore, the observed halting of reaction front can be attributed to the slim inner cavity, which cannot effectively reduce the reaction resistance. The halting of reaction front limits the charging capacity and charging rate of the battery. Present results suggest that the halting of reaction front can be overcome by increasing the inner radius of hollow nanowire in order to achieve a higher charging capacity.

As another example, Liu et al. studied the lithiation of an array of solid silicon nanowires and found it is difficult to fully lithiated the while solid silicon nanowires [33]. Based on this experimental observation, they predicted that hollow silicon nanotubes should be more favorably used as the anodes than the solid silicon nanowires [33]. Our calculations quantitatively justify their prediction: stress-associated resistance for lithiation in a hollow silicon nanowire can be much lower than that in a solid silicon nanowire, especially for hollow silicon nanowire with a larger inner radius. The relatively low lithiation resistance in hollow silicon nanowires makes them easier to be fully lithiated than solid ones, and thus the reduction of capacity due to partial lithiation can be avoided in hollow silicon nanowires. Therefore, hollow nanowire could be a candidate nanostructure for achieving high capacity in development of silicon anodes for lithium-ion batteries.

As indicated by Zhao et al. [25] and Liu et al. [33], since the stress evolution during lithiation arises from the curved reaction front,

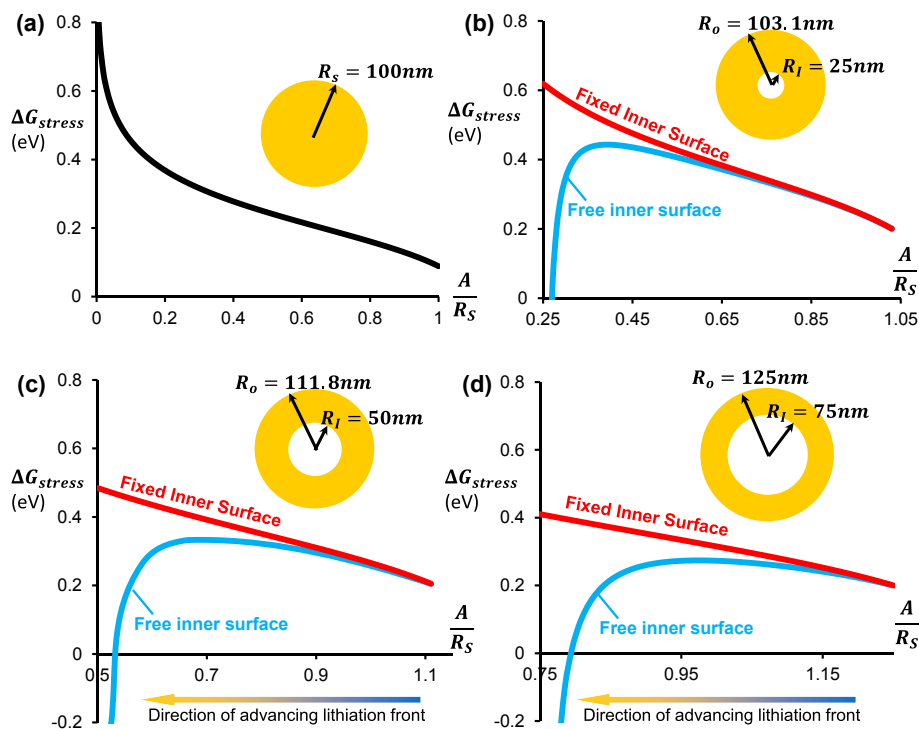


Fig. 5. Theoretical mechanics model results on stress-modulated driving force for lithiation as a function of the lithiation front position A/R_s , for (a) a solid silicon nanowire and (b–d) hollow silicon nanowires with normalized inner radius of (b) $R_i/R_s = 0.25$, (c) $R_i/R_s = 0.5$ and (d) $R_i/R_s = 0.75$, respectively. Blue lines in (b–d) represent the case of a hollow nanowire with a traction-free inner surface and red lines represent the case of a hollow nanowire with a fixed inner surface. (For interpretation of the references to color in this figure legend, the reader is referred to the web version of this article.)

the present results and conclusions are not limited to hollow nanowires, and can also be applicable to hollow nanoparticles. Yao et al. reported a structure of interconnected silicon hollow nanospheres as anodes for lithium-ion batteries [39]. The anode consists of spheres with an inner radius of ~ 175 nm and an outer radius of ~ 200 nm and demonstrates high discharging capacity over 700 cycles and superior rate capacity, which are attributed to the short lithium diffusion distance in the silicon hollow shell. Another possible explanation could be that the observed superior rate capacity is due to the low stress-modulated resistance for lithiation in hollow sphere: the inner radius (~ 175 nm) of the nanospheres is much larger than the shell thickness (~ 25 nm), therefore the stress-associated lithiation resistance can be significantly reduced, as predicted by the present model. Given that the velocity of the reaction front depends on the lithiation resistance, it is expected that hollow nanospheres can be lithiated faster than solid ones, as observed in hollow silicon nanospheres in Ref. [39]. Results from the present study together with the abovementioned related experimental observations offer insight on future development of silicon-based anodes for high performance lithium-ion batteries: hollow nanowires or nanospheres could serve as candidate designs of anodes with both high charging capacity and high charging rate.

5. Concluding remarks

This paper presents chemo-mechanical simulations and theoretical modeling to consider concurrent lithiation reaction and mechanical deformation in a hollow silicon nanowire anode as a sharp lithiation reaction front moves from the outer surface toward the inner surface of the hollow nanowire, from which the distribution and evolution of the lithiation-induced stress and its effect on the driving force for lithiation reaction in the nanowire anode are quantitatively determined. The lithiation-induced stress and

deformation fields in the hollow silicon nanowire are fully specified as functions of the position of the lithiation front and the boundary condition at the nanowire inner surface. In a solid silicon nanowire anode, lithiation-induced stress poses a resistance to the lithiation reaction, which increases monotonically as the lithiation front advances inward and could eventually overbalance the intrinsic driving force for lithiation reaction, causing a halt in the advancing lithiation front and leading to incomplete lithiation and thus lower charging capacity of the anode. By contrast, in a hollow silicon nanowire anode, the stress-associated resistance to the lithiation reaction is lower than that in a solid nanowire anode with the same volume. The difference in such a resistance between a hollow and a solid silicon nanowire becomes more substantial in the later stage of lithiation reaction. Interestingly, when the inner surface of the hollow silicon nanowire is free of mechanical constraint, the stress-associated resistance to the lithiation reaction peaks at an intermediate lithiation stage and then decreases. Toward the end of the lithiation stage, the lithiation-induced stress in a hollow silicon nanowire can even make an energetically favorable contribution to the driving force for lithiation reaction, that is, promote the advance of lithiation reaction front through the whole nanowire anode. Therefore, a hollow silicon nanowire anode is easier to be fully lithiated than its solid counterpart. Further study of the size effect on stress-modulated driving force for lithiation reaction reveals that a hollow nanowire with a larger inner radius and a free inner surface possesses lower stress-induced resistance to lithiation reaction and thus is a better anode design. It is hoped that these quantitative results can shed lights on optimal design of hollow silicon nano-anodes for high performance lithium-ion battery.

The present paper uses hollow cylindrical silicon nanowire anodes for lithium-ion battery as a model system to investigate stress-modulated driving force for electrochemical reaction in battery

anodes. The mechanics model as well as the mechanistic findings can be readily adapted to investigate anodes in other geometries (e.g., hollow spherical nanoparticles [39]), of other materials (e.g., germanium nano-anodes [46]), and even in other battery systems (e.g., sodium-ion battery [47–49]), given many similar features of reaction-induced deformation and stress in these different battery anodes as reported in recent experiments. Further studies along these directions, though beyond the scope of this paper, will be reported elsewhere.

Acknowledgments

ZJ and TL acknowledge the support by NSF Grants CMMI #1069076 and #1129826. ZJ also acknowledges the support from the Future Faculty Program in A. James Clark School of Engineering at the University of Maryland, College Park.

Appendix

A1. Stress distribution in the lithiated silicon shell ($A < r \leq r_0$)

In the current configuration at time t , consider a shell of silicon between the lithiation front A and radius r (Fig. 1(a), right panel), which results from the lithiation and deformation of a pristine silicon shell between radii A and R in the reference state (Fig. 1(a), left panel). Elongation of the silicon nanowire along its axial direction is expected to be negligible, thus the lithiated silicon in its cross section is assumed to deform under plane-strain conditions. Therefore, we have,

$$r^2 - A^2 = \beta(R^2 - A^2) \quad (\text{A.1})$$

where β is the volume expansion ratio defined by the volume of the lithiated silicon $Li_{3.75}Si$ over that of the pristine silicon. Eq. (A.1) relates the current coordinate $r(R, t)$ of a material point to its initial coordinate R and the current position of lithiation front $A(t)$, and can be re-organized as

$$r = \sqrt{A^2 + \beta(R^2 - A^2)} \quad (\text{A.2})$$

Eq. (A.2) determines the current configuration of the lithiated nanowire, where A acts as the only variable. Therefore, the current position of lithiation front $A(t)$ fully specifies the lithiation kinetics of the silicon nanowire anode.

The deformation kinematics of the silicon nanowire can be described by the deformation gradient tensor $\underline{\mathbf{F}}$ as follows:

$$\underline{\mathbf{F}} = \begin{bmatrix} \lambda_r & 0 & 0 \\ 0 & \lambda_\theta & 0 \\ 0 & 0 & \lambda_z \end{bmatrix} \quad (\text{A.3})$$

where hoop stretch $\lambda_\theta = r/R$ and axial stretch $\lambda_z = 1$ (plane-strain conditions). It is worth noting that during lithiation elastic strains are trivial compared with the large plastic and volumetric strains and thus are neglected. Therefore, the total deformation gradient tensor $\underline{\mathbf{F}}$ can be decomposed into a volumetric part and a plastic part as $\underline{\mathbf{F}} = \underline{\mathbf{F}}_v \underline{\mathbf{F}}_p$. The volume change of lithiated silicon is given by $\det(\underline{\mathbf{F}}) = \det(\underline{\mathbf{F}}_v) \det(\underline{\mathbf{F}}_p) = \det(\underline{\mathbf{F}}_v) = \beta$, entirely a result of lithiation-induced volume change, i.e., $\lambda_r \lambda_\theta \lambda_z = \beta$. The radial stretch is then calculated as $\lambda_r = (R/r)\beta$. Moreover, the lithiation-induced volume expansion is intrinsically isotropic and takes the following form:

$$\underline{\mathbf{F}}_v = \begin{bmatrix} \lambda_v & 0 & 0 \\ 0 & \lambda_v & 0 \\ 0 & 0 & \lambda_v \end{bmatrix} \quad (\text{A.4})$$

As abovementioned, $\det(\underline{\mathbf{F}}_v) = \beta$ and therefore $\lambda_v = \beta^{1/3}$. The deformation gradient tensor corresponding to plasticity is then given by

$$\underline{\mathbf{F}}_p = \underline{\mathbf{F}} \underline{\mathbf{F}}_v^{-1} = \begin{bmatrix} \lambda_r^p & 0 & 0 \\ 0 & \lambda_\theta^p & 0 \\ 0 & 0 & \lambda_z^p \end{bmatrix} = \begin{bmatrix} \frac{R}{r} \beta^{2/3} & 0 & 0 \\ 0 & \frac{r}{R} \beta^{-1/3} & 0 \\ 0 & 0 & \beta^{-1/3} \end{bmatrix} \quad (\text{A.5})$$

Given the relation between true strain and stretch ratio, the increment of true strain can be solved as

$$\delta \epsilon_r^p = (\beta - 1) A \delta A / r^2 \quad (\text{A.6.1})$$

$$\delta \epsilon_\theta^p = (1 - \beta) A \delta A / r^2 \quad (\text{A.6.2})$$

$$\delta \epsilon_z^p = 0 \quad (\text{A.6.3})$$

Eqs. (A.6.1–3) indicate that the deformation geometry of the lithiated silicon shell is fully evolved by the inward movement of the lithiation front ($\delta A < 0$). The increment of equivalent plastic strain is obtained as

$$\delta \epsilon_{eq}^p = \sqrt{\frac{2}{3} \delta \epsilon_{ij}^p \delta \epsilon_{ij}^p} = \frac{2}{\sqrt{3}} \frac{A |(1 - \beta) \delta A|}{r^2} = \frac{2}{\sqrt{3}} \frac{(1 - \beta) A \delta A}{r^2} \quad (\text{A.7})$$

The lithiated silicon is taken to be perfectly rigid plastic. According to the J_2 flow rule, the deviatoric stress components are solved as

$$s_r = \frac{2}{3} \frac{\sigma_Y}{\delta \epsilon_{eq}^p} \delta \epsilon_r^p = -\frac{\sigma_Y}{\sqrt{3}} \quad (\text{A.8.1})$$

$$s_\theta = \frac{\sigma_Y}{\sqrt{3}} \quad (\text{A.8.2})$$

$$s_z = 0 \quad (\text{A.8.3})$$

where σ_Y is the yielding stress of fully lithiated silicon $Li_{3.75}Si$. Therefore, we have

$$\sigma_r - \sigma_\theta = s_r - s_\theta = -\frac{2}{\sqrt{3}} \sigma_Y \quad (\text{A.9})$$

The equilibrium equation defined in the current configuration requires,

$$\frac{\partial \sigma_r(r, t)}{\partial r} + \frac{\sigma_r(r, t) - \sigma_\theta(r, t)}{r} = 0 \quad (\text{A.10})$$

where the boundary condition at the silicon nanowire surface $r = r_0$ is traction-free, i.e., $\sigma_r(r_0, t) = 0$. Plugging (A.9) into (A.10) and integrating over r give the radial stress in the lithiated shell ($A \leq r \leq r_0$):

$$\sigma_r = \frac{2}{\sqrt{3}} \sigma_Y \log \left(\frac{r}{r_0} \right), \quad (A < r \leq r_0) \quad (\text{A.11})$$

The hoop stress σ_θ inside the lithiated shell is then determined by Eq. (A.9)

$$\sigma_\theta = \frac{2}{\sqrt{3}}\sigma_Y + \frac{2}{\sqrt{3}}\sigma_Y \log\left(\frac{r}{r_0}\right), \quad (A < r \leq r_0) \quad (\text{A.12})$$

The axial stress is obtained from Eqs. (A.8.3), (A.11) and (A.12).

$$\sigma_z = \frac{1}{\sqrt{3}}\sigma_Y + \frac{2}{\sqrt{3}}\sigma_Y \log\left(\frac{r}{r_0}\right), \quad (A < r \leq r_0) \quad (\text{A.13})$$

A2. Stresses on the lithiation front ($r = A$)

For a material element right on the lithiation front characterized by $r = A$, lateral expansion (along axial and hoop directions) is strongly constrained by the inner unlithiated core. As a result, all stretch components can be written as

$$\lambda_r = \beta, \lambda_\theta = \lambda_\psi = 1. \quad (\text{A.14})$$

The plastic stretches at the lithiation reaction front are then given as

$$\lambda_r^p = \lambda_r \beta^{-1/3} = \beta^{2/3} \quad (\text{A.15.1})$$

$$\lambda_\theta^p = \lambda_\theta^p = \beta^{-1/3} \quad (\text{A.15.2})$$

On the lithiation front $r = A$, silicon reacts with lithium and eventually forms fully lithiated phase, $Li_{3.75}Si$. The associated volume expansion ratio β ramps from 1 (pristine state) to 4 (fully lithiated state) as the lithium concentration accumulates. Therefore, given a lithiation front at A , change of β evolves the plastic deformation at reaction front. Then, the increments of true strains are derived as

$$\delta \varepsilon_r^p = \frac{2}{3} \frac{\delta \beta}{\beta} \quad (\text{A.16.1})$$

$$\delta \varepsilon_\theta^p = \delta \varepsilon_\psi^p = -\frac{1}{3} \frac{\delta \beta}{\beta} \quad (\text{A.16.2})$$

The equivalent plastic strain is

$$\delta \varepsilon_{eq}^p = \sqrt{\frac{2}{3} \delta \varepsilon_{ij}^p \delta \varepsilon_{ij}^p} = \frac{2}{3} \frac{\delta \beta}{\beta} \quad (\text{A.17})$$

Therefore, the deviatoric stresses are

$$s_r = \frac{2}{3} \frac{\sigma_Y}{\delta \varepsilon_{eq}^p} \delta \varepsilon_r^p = \frac{2}{3} \sigma_Y \quad (\text{A.18.1})$$

$$s_\theta = s_z = -\frac{1}{3} \sigma_Y \quad (\text{A.18.2})$$

Radial stress σ_r is continuous across the lithiation front, therefore, at the lithiation front $r = A$,

$$\sigma_r = \frac{2}{\sqrt{3}}\sigma_Y \log\left(\frac{A}{r_0}\right) \quad (\text{A.19})$$

Eqs (A.18.1) and (A.18.2) indicate that $\sigma_r - \sigma_\theta = \sigma_Y$ and $\sigma_z = \sigma_\theta$, and we have

$$\sigma_\theta = -\sigma_Y + \frac{2}{\sqrt{3}}\sigma_Y \log\left(\frac{A}{r_0}\right) \quad (\text{A.20})$$

$$\sigma_z = -\sigma_Y + \frac{2}{\sqrt{3}}\sigma_Y \log\left(\frac{A}{r_0}\right) \quad (\text{A.21})$$

It is worth noting that the theoretical analysis in Sections A1 and A2 does not require any information about the unlithiated core, which indicates that stress evolutions in the lithiated shell and reaction front are not affected by the nature of unlithiated core (e.g., geometry, boundary conditions). Therefore, Eqs. (A.11–A.13) and (A.19–A.21) are also applicable for the stress evolution and distribution in the lithiated shell and on the reaction front for a solid silicon nanowire, respectively.

A3. Stress distribution in the remaining unlithiated hollow silicon shell ($R_l \leq r < A$)

The unlithiated hollow silicon part ($R_l \leq r < A$) is an annulus between radii R_l and A and subjected to a radial compression $2/\sqrt{3}\sigma_Y \log(r_0/A)$ at the lithiation reaction front. As discussed above, the inner surface of the remaining unlithiated silicon is either under fixed boundary condition (if the hollow nanowire is bonded to an inner constraint) or traction-free (if the hollow nanowire is free-standing). The stress field in the pristine unlithiated silicon can be obtained by solving a Lamé problem. For the traction-free inner surface, the stress field ($R_l \leq r < A$) is given as.

$$\sigma_r = \frac{2}{\sqrt{3}}\sigma_Y \log\left(\frac{A}{r_0}\right) \frac{A^2}{A^2 - R_l^2} \left(1 - \frac{R_l^2}{r^2}\right), \quad (R_l \leq r < A) \quad (\text{A.22.1})$$

$$\sigma_\theta = \frac{2}{\sqrt{3}}\sigma_Y \log\left(\frac{A}{r_0}\right) \frac{A^2}{A^2 - R_l^2} \left(1 + \frac{R_l^2}{r^2}\right), \quad (R_l \leq r < A) \quad (\text{A.22.2})$$

$$\sigma_z = \frac{4\nu}{\sqrt{3}}\sigma_Y \log\left(\frac{A}{r_0}\right) \frac{A^2}{A^2 - R_l^2}, \quad (R_l \leq r < A) \quad (\text{A.22.3})$$

Similarly, fixed boundary condition at the inner surface gives a stress field ($R_l \leq r < A$) as follows.

$$\sigma_r = \frac{2}{\sqrt{3}}\sigma_Y \log\left(\frac{A}{r_0}\right) \left[\frac{1}{\frac{r^2}{A^2} + \frac{1}{(1-2\nu)\frac{R_l^2}{R_l^2}}} + \frac{1}{\frac{(1-2\nu)R_l^2}{A^2} + 1} \right], \quad (R_l \leq r < A) \quad (\text{A.23.1})$$

$$\sigma_\theta = \frac{2}{\sqrt{3}}\sigma_Y \log\left(\frac{A}{r_0}\right) \left[-\frac{1}{\frac{r^2}{A^2} + \frac{1}{(1-2\nu)\frac{R_l^2}{R_l^2}}} + \frac{1}{\frac{(1-2\nu)R_l^2}{A^2} + 1} \right], \quad (R_l \leq r < A) \quad (\text{A.23.2})$$

$$\sigma_z = \frac{4\nu}{\sqrt{3}}\sigma_Y \log\left(\frac{A}{r_0}\right) \frac{1}{\frac{(1-2\nu)R_l^2}{A^2} + 1}, \quad (R_l \leq r < A) \quad (\text{A.23.3})$$

where ν is the Poisson's ratio of pristine amorphous silicon.

For a solid nanowire, the stress distribution in the unlithiated core can be derived by setting $R_l = 0$ in Eqs. (A.22.1–3):

$$\sigma_r = \frac{2}{\sqrt{3}}\sigma_Y \log\left(\frac{A}{r_0}\right), \quad (0 \leq r < A) \quad (\text{A.24.1})$$

$$\sigma_{\theta} = \frac{2}{\sqrt{3}} \sigma_Y \log \left(\frac{A}{r_0} \right), \quad (0 \leq r < A) \quad (\text{A.24.2})$$

$$\sigma_z = \frac{4\nu}{\sqrt{3}} \sigma_Y \log \left(\frac{A}{r_0} \right), \quad (0 \leq r < A) \quad (\text{A.24.3})$$

References

- [1] M. Armand, J.M. Tarascon, *Nature* 451 (2008) 652–657.
- [2] L.F. Cui, R. Ruffo, C.K. Chan, H. Peng, Y. Cui, *Nano Lett.* 9 (2009) 491–495.
- [3] D.K. Kim, P. Muralidharan, H.W. Lee, R. Ruffo, Y. Yang, C.K. Chan, H. Peng, R.A. Huggins, Y. Cui, *Nano Lett.* 8 (2008) 3948–3952.
- [4] I. Kovalenko, B. Zdyrko, A. Magasinski, B. Hertzberg, Z. Milicev, R. Burtovyy, I. Luzinov, G. Yushin, *Science* 334 (2011) 75–79.
- [5] R. Marom, S.F. Amalraj, N. Leifer, D. Jacob, D. Aurbach, *J. Mater. Chem.* 21 (2011) 9938–9954.
- [6] M.N. Obrovac, L. Christensen, *Electrochem. Solid State Lett.* 7 (2004) A93–A96.
- [7] M.N. Obrovac, L. Christensen, D.B. Le, J.R. Dahn, *J. Electrochem. Soc.* 154 (2007) A849–A855.
- [8] U. Kasavajjula, C. Wang, A.J. Appleby, *J. Power Sour.* 163 (2007) 1003–1039.
- [9] C.K. Chan, H. Peng, G. Liu, K. Mcllwraith, X.F. Zhang, R.A. Huggins, Y. Cui, *Nat. Nanotechnol.* 3 (2008) 31–35.
- [10] X.H. Liu, L. Zhong, S. Huang, S.X. Mao, T. Zhu, J.Y. Huang, *ACS Nano* 6 (2012) 1522–1531.
- [11] X.H. Liu, H. Zheng, L. Zhong, S. Huan, K. Karki, L.Q. Zhang, Y. Liu, A. Kushima, W.T. Liang, J.W. Wang, J.H. Cho, E. Epstein, S.A. Dayeh, S.T. Picraux, T. Zhu, J. Li, J.P. Sullivan, J. Cumings, C. Wang, S.X. Mao, Z.Z. Ye, S. Zhang, J.Y. Huang, *Nano Lett.* 11 (2011) 3312–3318.
- [12] K. Karki, E. Epstein, J.H. Cho, Z. Jia, T. Li, S.T. Picraux, C. Wang, J. Cumings, *Nano Lett.* 12 (2012) 1392–1397.
- [13] T. Takamura, S. Ohara, M. Uehara, J. Suzuki, K. Sekine, *J. Power Sour.* 129 (2004) 96–100.
- [14] L. Baggetto, D. Danilov, P.H.L. Notten, *Adv. Mater.* 23 (2011) 1563–1566.
- [15] H. Kim, B. Han, J. Choo, J. Cho, *Angew. Chem. Int. Ed.* 47 (2008) 10151–10154.
- [16] C.F. Sun, K. Karki, Z. Jia, H. Liao, Y. Zhang, T. Li, Y. Qi, J. Cumings, G.W. Rubloff, Y. Wang, *ACS Nano* 7 (2013) 2717–2724.
- [17] J. Wan, A.F. Kaplan, J. Zheng, X. Han, Y. Chen, N.J. Weadock, N. Faenza, S. Lacey, T. Li, J. Guo, L. Hu, *J. Mater. Chem. A* 2 (2014) 6051–6057.
- [18] H. Haftbaradaran, X. Xiao, M.W. Verbrugge, H. Gao, *J. Power Sour.* 206 (2012) 357–366.
- [19] S.K. Soni, B.W. Sheldon, X. Xiao, M.W. Verbrugge, D. Ahn, H. Haftbaradaran, H. Gao, *J. Electrochem. Soc.* 159 (2012) A38–A43.
- [20] V. Sethuraman, V. Srinivasan, A. Bower, P. Guduru, *J. Electrochem. Soc.* 157 (2010) A1253–A1261.
- [21] V. Sethuraman, N. Van Winkle, D. Abraham, A. Bower, P. Guduru, *J. Power Sour.* 206 (2012) 334–342.
- [22] V. Sethuraman, A. Nguyen, M. Chon, S. Nadimpalli, H. Wang, D. Abraham, A. Bower, V. Shenoy, P. Guduru, *J. Electrochem. Soc.* 160 (2013) A739–A746.
- [23] R.A. Huggins, W.D. Nix, *Ionics* 6 (2000) 57–63.
- [24] Y. Hu, X. Zhao, Z. Suo, *J. Mater. Res.* 25 (2010) 1007–1010.
- [25] K. Zhao, M. Pharr, Q. Wan, W.L. Wang, E. Kaxiras, J.J. Vlassak, Z. Suo, *J. Electrochem. Soc.* 159 (2012) A238–A243.
- [26] S. Huang, F. Fan, J. Li, S. Zhang, T. Zhu, *Acta Mater.* 61 (2013) 4354–4364.
- [27] H. Yang, S. Huang, X. Huang, F. Fan, W. Liang, X.H. Liu, L.Q. Chen, J.Y. Huang, J. Li, T. Zhu, S. Zhang, *Nano Lett.* 12 (2012) 1953–1958.
- [28] A. Bower, P. Guduru, V. Sethuraman, *J. Mech. Phys. Solids* 59 (2011) 804–828.
- [29] J. Christensen, J. Newman, *J. Solid State Electrochem.* 10 (2006) 293–319.
- [30] Y.F. Gao, M. Zhou, *J. Power Sour.* 230 (2013) 176–193.
- [31] K. Zhao, M. Pharr, L. Hartle, J.J. Vlassak, Z. Suo, *J. Power Sour.* 218 (2012) 6–14.
- [32] M. McDowell, I. Ryu, S. Lee, C. Wang, W. Nix, Y. Cui, *Adv. Mater.* 24 (2012) 6034–6041.
- [33] X. Liu, F. Fan, H. Yang, S. Zhang, J. Huang, T. Zhu, *ACS Nano* 7 (2013) 1495–1503.
- [34] X. Liu, J. Wang, S. Huang, F. Fan, X. Huang, Y. Liu, S. Krylyuk, J. Yoo, S. Dayeh, A. Davydov, S. Mao, S. Picraux, S. Zhang, J. Li, T. Zhu, J. Huang, *Nat. Nanotechnol.* 7 (2012) 749–756.
- [35] B. Key, R. Bhattacharyya, M. Morcrette, V. Seznec, J. Tarascon, C. Grey, *J. Am. Chem. Soc.* 131 (2009) 9239–9249.
- [36] B. Key, M. Morcrette, J. Tarascon, C. Grey, *J. Am. Chem. Soc.* 133 (2011) 503–512.
- [37] Y.F. Gao, M. Zhou, *Acta Mech. Sin.* 28 (2012) 1068–1077.
- [38] Y.F. Gao, M. Zhou, *J. Appl. Phys.* 109 (2011) 014310.
- [39] Y. Yao, M.T. McDowell, I. Ryu, H. Wu, N. Liu, L. Hu, W.D. Nix, Y. Cui, *Nano Lett.* 11 (2011) 2949–2954.
- [40] N. Liu, H. Wu, M.T. McDowell, Y. Yao, C. Wang, Y. Cui, *Nano Lett.* 12 (2012) 3315–3321.
- [41] N. Yan, F. Wang, H. Zhong, Y. Li, Y. Wang, L. Hu, Q. Chen, *Sci. Rep.* 3 (2013).
- [42] D. Chen, X. Mei, G. Ji, M. Lu, J. Xie, J. Lu, J.Y. Lee, *Angew. Chem. Int. Ed.* 51 (2012) 2409–2413.
- [43] A. Magasinski, P. Dixon, B. Hertzberg, A. Kvit, J. Ayala, G. Yushin, *Nat. Mater.* 9 (2010) 353–358.
- [44] V.A. Sethuraman, M.J. Chon, M. Shimshak, V. Srinivasan, P.R. Guduru, *J. Power Sour.* 195 (2010) 5062–5066.
- [45] S.W. Lee, M.T. McDowell, L.A. Berla, W.D. Nix, Y. Cui, *Proc. Natl. Acad. Sci. U. S. A.* 109 (2012) 4080–4085.
- [46] W.T. Liang, H. Yang, F.F. Fan, Y. Liu, X.H. Liu, J.Y. Huang, T. Zhu, S.L. Zhang, *ACS Nano* 7 (2013) 3427–3433.
- [47] H. Zhu, Z. Jia, Y. Chen, N. Weadock, J. Wan, O. Vaaland, X. Han, T. Li, L. Hu, *Nano Lett.* 13 (2013) 3093–3100.
- [48] V. Palomares, P. Serras, I. Villaluenga, K.B. Hueso, J. Carretero-Gonzalez, T. Rojo, *Energy Environ. Sci.* 5 (2012) 5884–5901.
- [49] X. Han, Y. Liu, Z. Jia, Y.C. Chen, J. Wan, N. Weadock, K.J. Gaskell, T. Li, L. Hu, *Nano Lett.* 14 (2014) 139–147.